Applied Catalysis B: Environmental 181 (2016) 625–634

Contents lists available at ScienceDirect

Applied Catalysis B: Environmental

journal homepage: www.elsevier.com/locate/apcatb

The pivotal effect of the interaction between reactant and anatase TiO_2 nanosheets with exposed {0 0 1} facets on photocatalysis for the photocatalytic purification of VOCs

Lu Ren, Yuanzhi Li*, Jingtao Hou, Jilin Bai, Mingyang Mao, Min Zeng, Xiujian Zhao, Neng Li

State Key Laboratory of Silicate Materials for Architectures, Wuhan University of Technology, 122 Luoshi Road, Wuhan 430070, PR China

ARTICLE INFO

Article history:
Received 9 July 2015
Received in revised form 11 August 2015
Accepted 15 August 2015
Available online 20 August 2015

Keywords:
Photodegradation of VOCs
Anatase TiO_2 nanosheets
{0 0 1} facets
Interaction

ABSTRACT

We study the effect of the interaction between reactants and F-free or F-modified anatase TiO_2 nanosheets with exposed {0 0 1} facets on photocatalysis. It is found for the first time that the strong interaction between the reactants and TiO_2 nanosheets not only reverses the photocatalytic activity of the F-free TiO_2 nanosheets and F-modified TiO_2 nanosheets, but also conspicuously induces efficient visible photocatalytic activity for the photodegradation of VOCs such as acetone, benzene, and toluene in spite of the large band gap of anatase TiO_2 (3.2 eV) and no absorption of the VOCs in visible region. F-modified TiO_2 nanosheets have more strong interaction with acetone than F-free TiO_2 nanosheets, resulting in the photocatalytic activity of the former higher than the later and the visible photocatalytic activity of the former for the acetone photodegradation. On the other hand, F-free TiO_2 nanosheets have more strong interaction with benzene or toluene than F-modified TiO_2 nanosheets, resulting in the photocatalytic activity of the former higher than the later and the visible photocatalytic activity of the former for the photodegradation of benzene or toluene. We provide a fundamental insight in the novel and important effect of the interaction on the basis of both DFT calculation and the experimental evidences by photocurrent measurement and fluorescence emission decay. The strong interaction affects both the separation efficiency of the photogenerated charge carriers from TiO_2 to the reactants and their band gap characteristics.

1. Introduction

Volatile organic compounds (VOCs), which are major air pollutants in indoor air and polluted urban atmosphere, are harmful to both human health and the environment. Photodegradation based on nanostructured TiO_2 is a promising method for VOCs abatement because of its superior photocatalytic activity, chemical stability, low cost, and nontoxicity [1]. However, its photoactivation only by UV light owing to its large band gap and low quantum efficiency due to the fast recombination of photogenerated charge carriers hinder its wide application [1,2]. It is significant and challenging to develop novel strategies of improving its photocatalytic efficiency and extending its response to visible region. This ambition could be implemented on the basis of understanding its photocatalysis mechanism in depth [1–3]: Upon excitation of TiO_2 by photons with energy equal to or greater than its band gap, electrons are excited from the valence band to the conduction band. The photogenerated electrons (e) and holes (h) migrate from bulk to surface, where electrons reduce adsorbed electron acceptor (e.g., O_2) and holes oxidize adsorbed donor species (e.g., organic reactants or hydroxyl). In principle, the interaction between the adsorbed reactants and TiO_2 may play crucial role in photocatalysis as it can affect the charge transfer from TiO_2 to the adsorbed reactants, thus affecting the e–h separation efficiency and photocatalytic activity. The interaction depends on the property of the reactant as well as the surface physicochemical property of TiO_2 nanocrystals. However, few works about the effect of the interaction between the adsorbed reactants and TiO_2 on photocatalysis have been reported.

Recently, there have been enormous interests in anatase TiO_2 nanocrystal with dominant {0 0 1} facets due to its fascinating physicochemical properties such as active unsaturated Ti atoms, high surface energy, etc., [4–28], since Yang et al. reported the synthesis of anatase TiO_2 single crystals with high percentage of exposed {0 0 1} facets by using F^- as a stabilizing agent [4]. Most of the reported works about the photocatalysis of anatase TiO_2 nanocrystal with exposed {0 0 1} facets focus on the effect of

* Corresponding author. Fax: +86 27 87883743.
E-mail address: liyuanzhi66@hotmail.com (Y. Li).

http://dx.doi.org/10.1016/j.apcatb.2015.08.034
0926-3373/

high energy {0 0 1} facet on the liquid-phase photodegradation of organic pollutants, the gas-phase photodegradation of VOCs, and photocatalytic production of fuels (e.g., H_2) [5–28]. To our best knowledge, there have been no reports on the visible photocatalytic activity of anatase TiO_2 nanocrystal with exposed {0 0 1} facets for the gas-phase photodegradation of VOCs owing to its large band gap (3.2 eV). Because of the active unsaturated Ti atoms and high surface energy of the {0 0 1} facets of anatase TiO_2, it is expected that there is stronger interaction between the adsorbed reactants and anatase TiO_2 nanocrystal with exposed {0 0 1} facets. This strong interaction may induce the unexpected photocatalytic property for anatase TiO_2 nanocrystal with exposed {0 0 1} facets. For example, Sun et al. investigated the adsorption of oxalic acid on anatase TiO_2 {0 0 1} surface by density functional theory, and concluded that oxalic acid preferred the dissociative adsorption on the anatase {0 0 1} surface with the double-bidentate configuration, in which more charge was transferred from the adsorbed oxalic acid to the anatase {0 0 1} surface [29].

Herein, we report a novel and important effect of the interaction between reactant and TiO_2 nanosheets with exposed {0 0 1} facets on photocatalysis. It is found for the first time that the strong interaction between VOCs (e.g., acetone, benzene, toluene) and the TiO_2 nanosheets not only reverses the photocatalytic activity of F-free TiO_2 nanosheets and F-modified TiO_2 nanosheets, but also conspicuously induces efficient visible photocatalytic activity in spite of the large band gap of anatase TiO_2 (3.2 eV) and no absorption of the VOCs in visible region. We provide a fundamental insight in the effect of the interaction on the basis of DFT calculation and experimental evidence.

2. Experimental

2.1. Preparation

Anatase TiO_2 nanosheets with dominant {0 0 1} facets were prepared by the hydrothermal reaction of $Ti(OBu)_4$ in the presence of HF at 180 °C according to the procedure reported by Yu et al. [30]. The obtained sample is denoted as TNS-F. The TNS-F powder was washed with 0.1 mol L^{-1} NaOH aqueous solution and distilled water respectively for three times to remove fluorine in the TNS-F powder, filtered, and dried in an oven at 80 °C for 6 h. The obtained TiO_2 sample is denoted as TNS.

2.2. Characterization

XRD patterns were taken on a Rigaku Dmax X-ray diffractometer using Cu Kα radiation. SEM images were observed on a Hitachi S-4800 scanning electron microscope. TEM images were observed on a JEM-100CX electron microscope. The BET surface area was measured on AUTOSORB-1 using N_2 adsorption at −196 °C. The valence state of the elements in the samples was analysed on a VG Multilab 2000 X-ray photoelectron spectrometer (XPS) using Al Kα source. Diffuse reflectance UV–vis (DRUV–vis) absorption was measured on a UV-3600 spectrophotometer. In order to measure the UV–vis spectra of the TiO_2 samples before and after the adsorption of benzene or acetone, the UV–vis spectra of the TiO_2 samples in air was first recorded. Then 100 mL of acetone or benzene saturated air was injected into the integral sphere chamber where the TiO_2 sample was placed, and the UV–vis spectra of the TiO_2 samples in the vapor of benzene or acetone was recorded again.

The transient response of photocurrent for the ITO/TiO_2 film/ITO stack in different atmosphere at ambient temperature was recorded under an operation voltage of 0.5 V on an electrochemical analyzer (CHI750). The ITO/TiO_2 film/ITO stack was prepared according to the procedure reported in our previous work [31]. The stack was placed on the bottom of a closed cylindrical stainless steel reactor (710 mL) with a quartz window. An 80 W high pressure Hg lamp was used as a light source. After measuring the photocurrent of the TiO_2 samples in air, 60 mL of acetone or benzene saturated air was injected into the reactor from an injection pore sealed with silicone rubber.

The steady-state fluorescence and fluorescence emission decay for the TiO_2 samples in different atmosphere were conducted at ambient temperature on a QM/TM/NIR spectrofluorometer (PTI) with 337 nm excitation light. The TiO_2 sample was put in a closed powder holder. After measuring the fluorescence emission decay of the TiO_2 samples in air, 10 mL of acetone or benzene saturated air was injected into the holder.

2.3. Photocatalytic activity

The catalytic activity of the TiO_2 photocatalyst for the gas-phase photodegradation of acetone, benzene, and toluene was tested on a closed cylindrical stainless gas-phase batch reactor with a volume of 7.2 L. An 80 W high pressure Hg lamp as light source was fixed on the inner wall of the reactor. 0.5000 g of the TiO_2 powder was dispersed on a glass dish, and set on the bottom of the reactor. The reactor was put in an ice-water bath to maintain the reaction temperature at near room temperature (~40 °C). The intensity of UV light (320–400 nm) from the Hg lamp was measured by an UV-A Radiometer (4.97 mW cm^{-2}). The intensity of visible light (400–1000 nm) from the Hg lamp was measured by a FZ-A Radiometer (15.04 mW cm^{-2}). 5 μL acetone or 2 μL benzene or toluene was injected into the reactor. Reactants and products were analyzed on a GC9560 gas chromatograph. The details of GC analysis condition are described in our previous works [32,33]. To measure the photocatalytic activity of the TiO_2 samples under the visible irradiation, a cutoff filter of 420 nm, 480 nm, or 560 nm was put between the Hg lamp and the TiO_2 powder in the reactor.

2.4. DFT calculation

The DFT calculation was performed using the Vienna Ab-initio Simulation package (version VASP 5.3) [34–37]. The valence electronic states are expanded in a set of periodic plane waves, and the interaction between the core electrons and valence electrons is implemented through the projector augmented wave (PAW) approach. The Perdew–Burke–Ernzerhof (PBE) GGA-exchange correlation functional is applied in the calculations [32,33,35]. The smooth part of the wave functions is expanded in plane waves with a kinetic energy cutoff of 400 eV, and the convergence criteria for the electronic and ionic relaxation are 10^{-4} eV and 0.02 eV $Å^{-1}$, respectively [32,33]. A slab $Ti_{27}O_{54}$ of three TiO_2 layers and a 3×3 {0 0 1} surface cell with anatase structure was employed as model in the calculation. The space between neighboring {001} surfaces of the slabs was 1.5 nm. In relaxation, summation over the Brillouin zone was performed by a $2 \times 2 \times 2$ Monkhorst–Pack k-point mesh for the structure optimization. For the calculation of density of states (DOS), summation over the Brillouin zone was performed by a $6 \times 6 \times 6$ Monkhorst–Pack k-point mesh based on the structure optimized systems. The adsorption energy of organic molecule on the TiO_2 slab is defined as:

$$\Delta E = E_{OT} - E_T - E_O$$

where E_{OT} is the energy of organic molecule adsorbed on the TiO_2 slab, E_T is the energy of the TiO_2 slab, and E_O is the energy of free organic molecule.

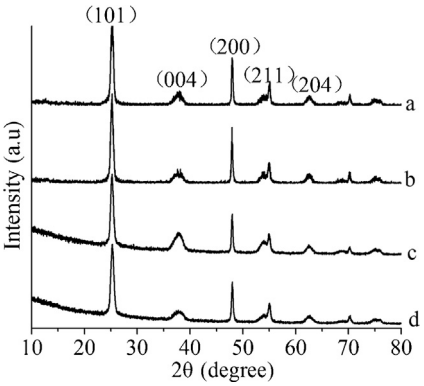

Fig. 1. XRD patterns of the TNS-F (a), TNS (b), the used TNS-F (c) and TNS (d).

3. Resutls and discussion

3.1. Characterization

Anatase TiO_2 nanosheets with dominant {0 0 1} facets were prepared by the hydrothermal reaction of $Ti(OBu)_4$ in the presence of HF at 180 °C according to the procedure reported by Yu et al. [30]. The obtained TiO_2 sample is denoted as TNS-F. XRD reveals that TNS-F has pure anatase structure (PDF 04-0477) (Fig. 1). The narrow {2 0 0} peak as well as broad {0 0 4} peak as shown in Fig. 1 indicates that the crystal growth is limited primarily to the [0 0 1] axis, resulting in the dominant {001} facets [17]. The average thickness and length of the TiO_2 nanosheets corresponding to {0 0 4} and {2 0 0} facets, which are determined by using the Scherrer formula ($L = 0.89\lambda/\beta \cos\theta$), are 6.5, 34 nm, respectively. The percentage of the exposed {0 0 1} facets in TNS-F is estimated by the average thickness and length to be 72.3 %. SEM and TEM images confirm that TNS-F has morphology of nanosheets with dominant {0 0 1} facets (Fig. 2). The average percentage of the exposed {0 0 1} facets in TNS-F is also estimated by measuring the thickness and length of TiO_2 nanosheets in Fig. 3B (HRTEM) to be 74.5%, which is generally in agreement with that by XRD. XPS reveals the presence of F (F/Ti molar ratio = 0.32) in TNS-F in the form of surface fluoride (Ti–F) (Fig. 3), evidenced by the fact that F1s peak at 684.0 eV is observed and no F in the lattice of TiO_2 (688.5 eV) is detected [30]. The peak is at 832.0 eV (Fig. 3A), which is assigned to the F KLL Auger peak of the surface fluoride (Ti-F) in TNS-F [10]. N_2 adsorption–desorption experiment shows that the BET surface area of TNS-F is 95.7 $m^2\ g^{-1}$ (Fig. S1).

F-free anatase TiO_2 nanosheets, denoted as TNS, were prepared by washing TNS-F with 0.1 M NaOH aqueous solution, and then with distilled water. XRD, SEM, and TEM reveal that the washing does not change its crystallinity and morphology (Figs. 1 and 2). XPS confirms that the surface F is removed by the washing and Na^+ is not detected in the TNS (Fig. 3). The BET surface area of TNS is 113.1 $m^2\ g^{-1}$.

3.2. Photocatalytic activity

The photocatalytic activity of TNS-F and TNS was studied by evaluating the rate of CO_2 production from the photodegradation of acetone and benzene as typical polar and nonpolar reactants of volatile organic contaminants, respectively, under the irradiation of the Hg lamp. For the acetone photodegradation, TNS-F exhibits higher photocatalytic activity than TNS (Fig. 4A). The CO_2 production rate of TNS-F (10.19 $\mu mol\ g^{-1}_{\text{-catalyst}}\ min^{-1}$) is 1.3 times higher than that of TNS. As TNS-F and TNS have different surface area, we compare their specific rates of CO_2 production per unit surface area of photocatalyst. The specific rate of CO_2 production of TNS-F (0.106 $\mu mol\ m^{-2}_{\text{-catalyst}}\ min^{-1}$) is 1.6 times higher than that of TNS. The higher photocatalytic activity of TNS-F than TNS is attributed to the surface fluorination of TiO_2 nanosheets, which is in accordance with the results for both liquid-phase and gas-phase photodegradation reported by several research groups [30,31,38–44]. TNS-F and TNS may have different amount of surface hydroxyl group that may influence their photocatalytic activity. The amount of surface hydroxyl group on the TiO_2 samples can be changed by humidity, which is also a key factor in the photodegradation of VOCs. To confirm whether the photocatalytic enhancement is attributed to the surface fluorination of TiO_2 nanosheets, we measured the photocatalytic activity of TNS-F and TNS for acetone photodegradation under higher relative humidity adjusted by injecting water into the reactor. As can be seen from Fig. 4 and Fig. S2, increasing the relative humidity from 60% (Fig. 4) to 100% leads to an enhancement of photocatalytic activity for both TNS-F and TNS. But, TNS-F still exhibits higher photocatalytic activity than TNS under the higher relative humidity (Fig. S2). The result clearly suggests that the higher photocatalytic activity of TNS-F than TNS is due to the surface fluorination of TiO_2 nanosheets rather than the effect of surface hydroxyl groups.

The widely accepted explanation to the photocatalytic enhancement by the surface fluorination of TiO_2 is as follows: the surface fluorination of TiO_2 promotes the production of mobile free •OH radicals by oxidizing adsorbed H_2O, whereas most •OH radicals generated on pure TiO_2 surface prefer to remain adsorbed [38–42]. The desorbed and free •OH radicals are more reactive than the surface-bound •OH owing to the facile homogeneous photocatalyticreactions [38,42]. Recently, Luan et al. provided another explanation: the surface modification of TiO_2 with F or phosphate could greatly enhance the adsorption of O_2 so as to promote the photogenerated electrons captured by the adsorbed O_2, leading to the great increase in the charge separation and then in the photocatalytic activity [44]. According to these explanations, the photocatalytic enhancement by the surface fluorination of TiO_2 is independent of organic reactants. The F-modified TiO_2 nanosheets (TNS-F) should have higher photocatalytic activity for the photodegradation of any organic compounds than the F-free TiO_2 nanosheets (TNS). Unexpectedly, for the photodegradation of benzene, TNS-F exhibits much lower photocatalytic activity than TNS (Fig. 4B). This is in striking contrast to the observation in the acetone photodegradation. The rate of CO_2 production of TNS (1.98 $\mu mol\ g^{-1}_{\text{-catalyst}}\ min^{-1}$) is 4.4 times higher than that of TNS-F. The reverse photocatalytic activity of TNS-F and TNS for the benzene photodegradation compared to the acetone photodegradation reveals that there is a novel effect of the interaction between the reactants and TiO_2 nanosheets on photocatalysis.

More conspicuously, the interaction between the reactants and TiO_2 nanosheets induces efficient visible photocatalytic activity, although the reactants (e.g., acetone, benzene) and TiO_2 nanosheets have no absorption in visible region. For the acetone photodegradation, TNS-F exhibits very good photocatalytic activity under the visible irradiation above 420 and 480 nm (Fig. 4C), and their corresponding rate of CO_2 production is 2.85, 1.90 $\mu mol\ g^{-1}_{\text{-catalyst}}\ min^{-1}$, respectively. Even under the visible irradiation above 560 nm, acetone is efficiently photodegraded on TNS-F, and its rate of CO_2 production is 1.64 $\mu mol\ g^{-1}_{\text{-catalyst}}\ min^{-1}$. For benzene photodegradation, TNS exhibits efficient photocatalytic activity under the visible irradiation above 420 nm, and the rate of CO_2 production is 0.63 $\mu mol\ g^{-1}_{\text{-catalyst}}\ min^{-1}$. Under the visible irradiation above 480 nm, benzene is still photodegraded on TNS (Fig. 4D).

Similar phenomena for the toluene photodegradation on TNS and TNS-F are observed. TNS exhibits higher photocatalytic activity than TNS-F under the UV irradiation and shows photocatalytic

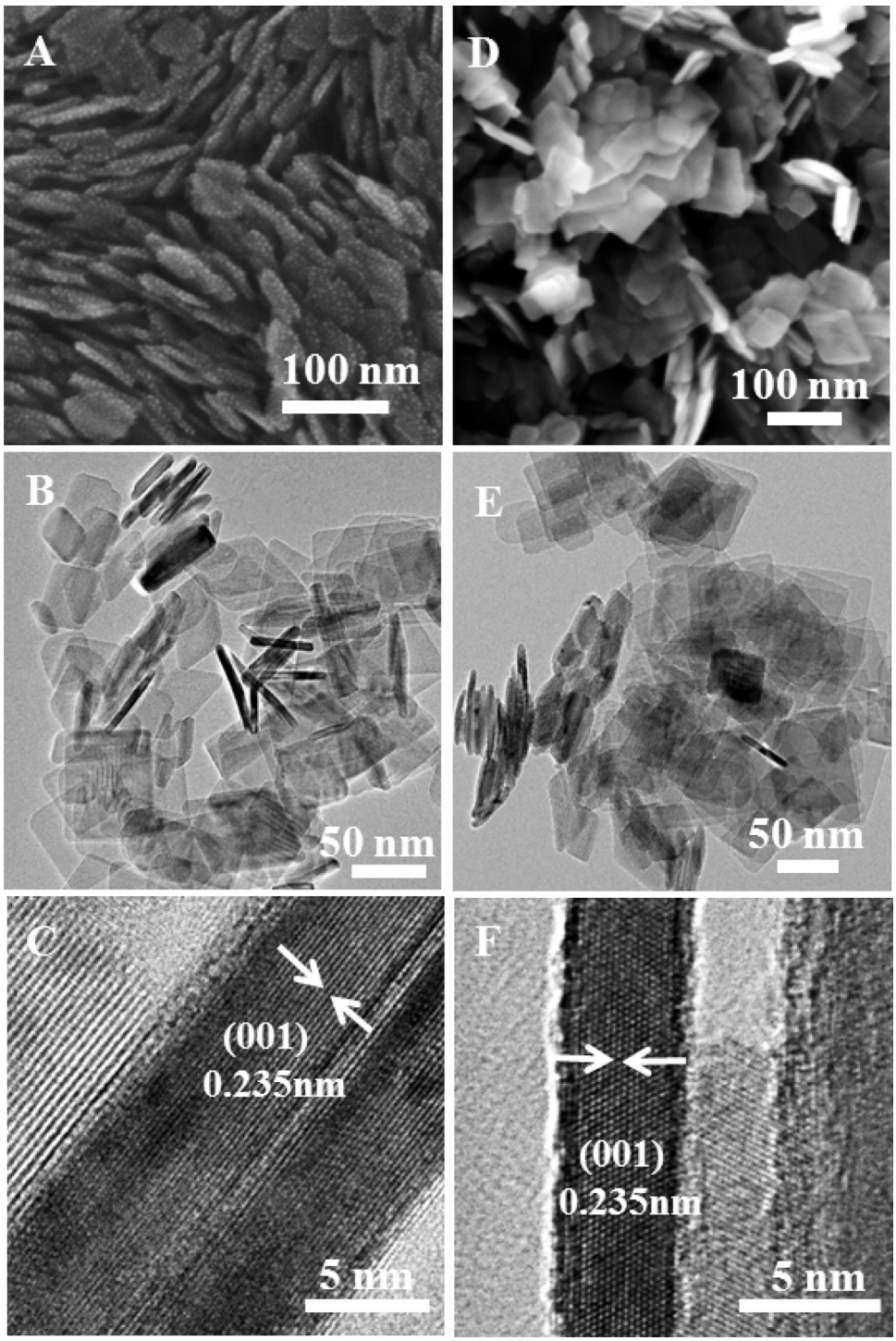

Fig. 2. SEM, TEM, and HRTEM image from the vertical nanosheet: TNS-F (A–C) and TNS (D–F).

activity under the visible irradiation above 420 nm (Fig. S3). These results clearly reveal that the strong interaction between the reactants and {0 0 1} facets of anatase TiO_2 plays a crucial role in the photocatalysis.

We measured the photocatalytic stability of TNS-F and TNS for benzene photodegradation. Both TNS-F and TNS show good photocatalytic stability after they are recycled for 20 times (Fig. S4). After the recycled test, the used TNS-F sample was characterized by XRD and XPS. XRD reveals that their anatase crystalline structure remains unchanged after the recycled test (Fig. 1). XPS reveals the presence of F in the form of surface fluoride in the used TNS-F evidenced by F1s peak at 684.0 eV (Fig. 3) [30]. But its F/Ti molar ratio decreases to 0.23 as compared to that of the fresh TNS-F (0.32), suggesting that some surface F on TNS-F is decomposed in the photocatalytic degradation process.

3.3. Photocurrent and UV–vis absorption.

It is well known that the e–h separation efficiency plays a crucial role in photocatalysis [45,46]: high e–h separation efficiency results in a high photocatalytic activity. Therefore, to reveal the origin of the interaction between the reactants and TiO_2 nanosheets on

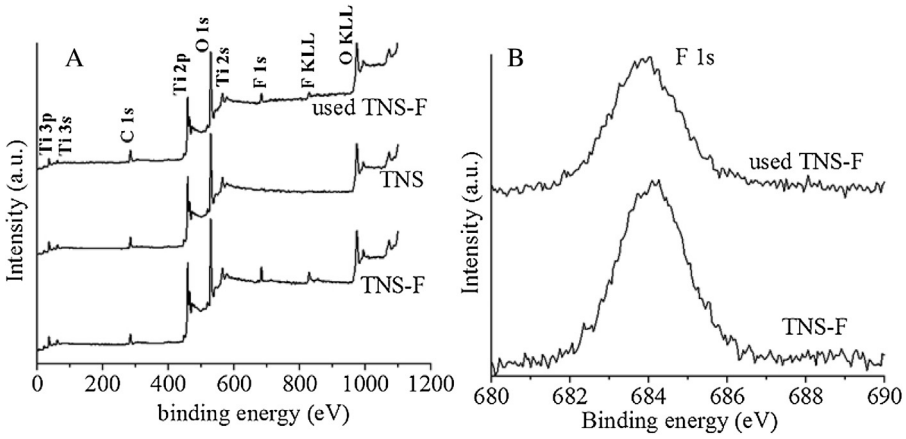

Fig. 3. XPS spectra of TNS-F, TNS, and the used TNS-F (A), and F1s XPS spectra of TNS-F and the used TNS-F (B).

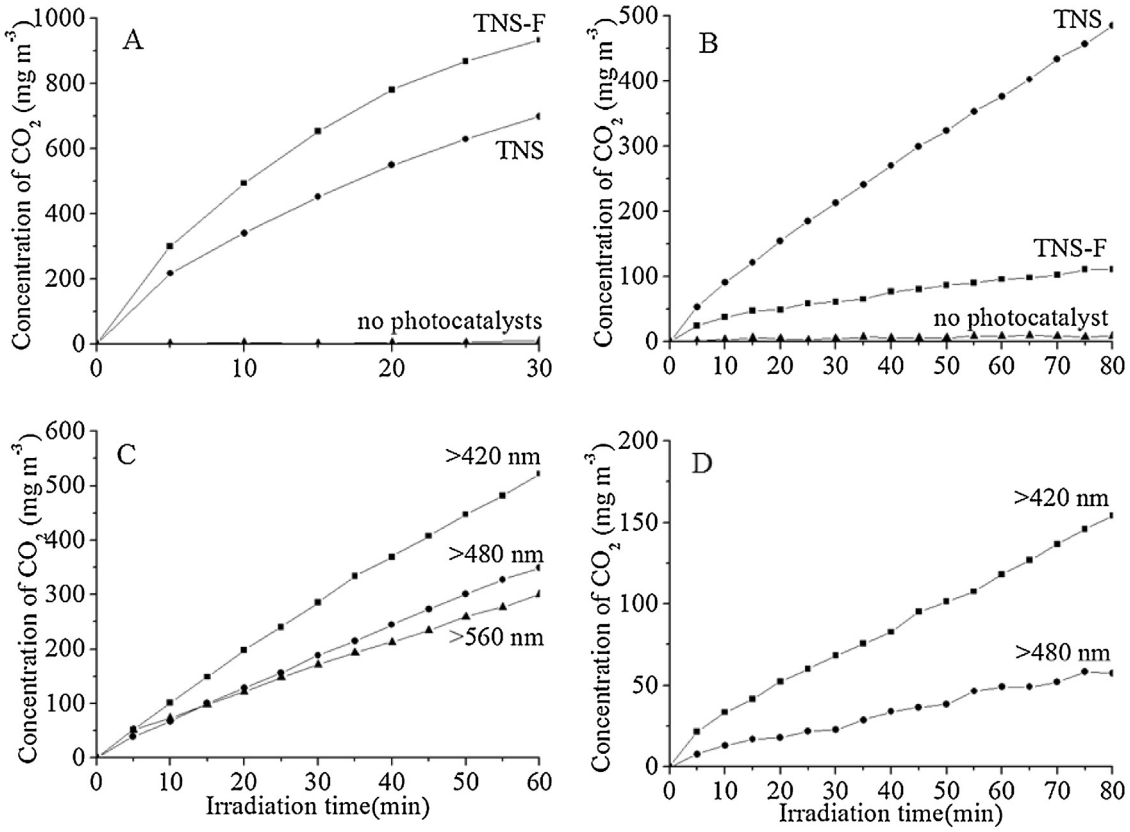

Fig. 4. Time course of CO_2 produced for the photodegradation of acetone (A) and benzene (B) on TNS-F and TNS under 60% relative humidity with the irradiation of the Hg lamp, and time course of CO_2 produced for the photodegradation of acetone on TNS-F (C) and benzene on TNS (D) under the visible irradiation using different cut-off filter.

photocatalysis, the photocurrent of TNS-F and TNS was measured in the different atmosphere to characterize the e–h separation efficiency (Fig. 5). Under the UV irradiation, the maximum photocurrent of TNS-F in air is much larger than that of TNS, indicating the higher e–h separation efficiency of TNS-F than TNS. When the atmosphere changes from air to acetone vapor, the maximum photocurrent of TNS-F increases (Fig. 5A). In contrast, the maximum photocurrent of TNS decreases (Fig. 5B). This result suggests that the strong interaction between acetone and TNS-F considerably increases the e–h separation efficiency. The e–h separation efficiency of TNS-F higher than TNS in acetone vapor results in its higher photocatalytic activity for acetone photodegradation (Fig. 4A). Interestingly, when the atmosphere changes from air to benzene vapor, a reverse evolution of photocurrent for TNS-F and TNS as compared to the observation in acetone vapor is observed. The maximum photocurrent of TNS-F decreases (Fig. 5A), while the maximum photocurrent of TNS increases (Fig. 5B). This result indicates that the strong interaction between benzene and TNS significantly increases its e–h separation efficiency, thus increasing the photocatalytic activity of TNS for the benzene photodegradation (Fig. 4B).

We measured the photocurrent of TNS-F in acetone vapor under visible irradiation. TNS-F exhibits photocurrent response under the visible irradiation above 420 nm (Fig. 5A), which is attributed to the enhancement of the visible absorption above 420 nm after the adsorption of acetone on TNS-F (Fig. 5C). This explains why TNS-F exhibits efficient photocatalytic activity for the acetone photodegradation with the visible irradiation (Fig. 4C). This result

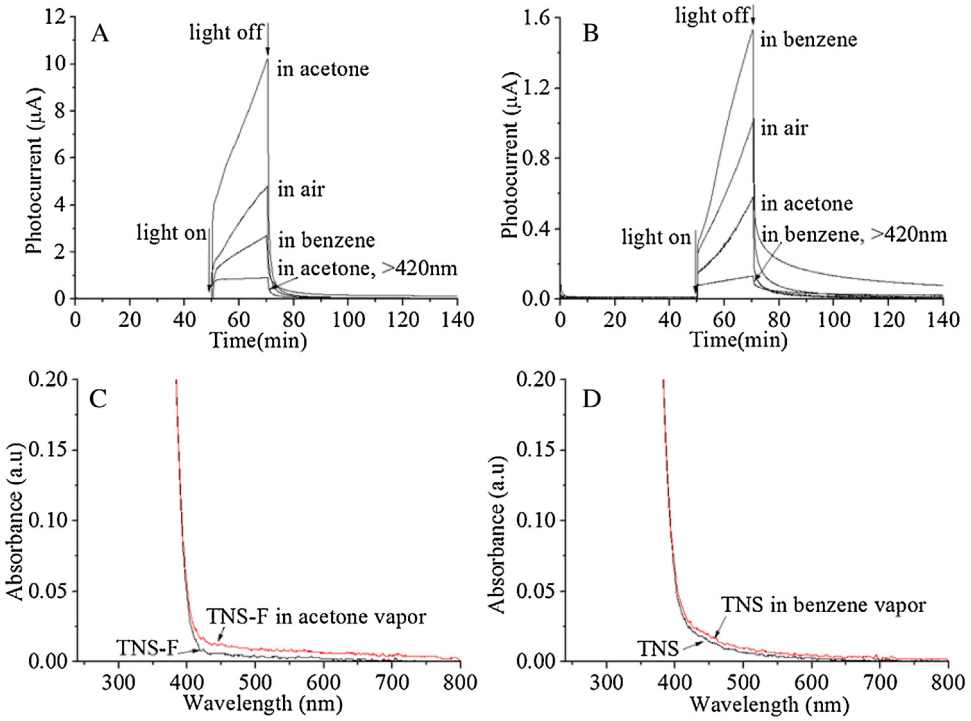

Fig. 5. Transient response of the photocurrent for TNS-F (A) and TNS (B) in different atmosphere under the irradiation of UV light and visible light above 420 nm. DRUV–vis spectra of TNS-F in air and in acetone vapor (C), and TNS in air and in benzene vapor (D).

suggests the presence of a strong interaction between acetone and F-modified TiO_2 nanosheets. The photocurrent of TNS in benzene vapor under visible irradiation was also measured. TNS exhibits photocurrent response under the visible irradiation above 420 nm (Fig. 5B), which is attributed to the slight enhancement of the visible absorption after the adsorption of benzene on TNS (Fig. 5D). The visible absorption and visible photocurrent response of TNS in benzene vapor result in its visible photocatalytic activity for the benzene photodegradation (Fig. 4D). This result suggests the presence of a strong interaction between benzene and F-free TiO_2 nanosheets.

3.4. Fluorescence emission decay

To further reveal the origin of the reverse photocatalytic activity of TNS-F and TNS for the benzene photodegradation as compared to the acetone photodegradation, the recombination dynamics of photogenerated e–h for the two TiO_2 samples in different atmosphere is studied by fluorescence emission decay (FED) using 337 nm excitation light. The steady-state fluorescence spectra show that the maximum fluorescence of TNS-F appears around 430 nm (Fig. S5). Thus, FED of the TiO_2 samples is recorded at 430 nm. The FED curve is fitted with a single-exponential curve (Fig. 6). When the atmosphere changes from air to acetone vapor, the fluorescence lifetime of both TNS-F and TNS almost remains unchanged. TNS-F has a fluorescence lifetime (2.633 ns) longer than the TNS (2.399 ns) in acetone vapor, indicating that the photogenerated e–h in the former has more probability to migrate from bulk to surface, where they participate in the photodegradation reaction of acetone. This result further provides evidence why TNS-F exhibits higher photocatalytic activity for the acetone photodegradation (Fig. 4A). Interestingly, when the atmosphere changes from air to benzene vapor, the fluorescence lifetime of TNS-F decreases from 2.604 ns to 2.500 ns (Fig. 6A). Remarkably, the fluorescence lifetime of TNS increases from 2.418 ns to 2.648 ns (Fig. 6B). This result indicates that the interaction between benzene and TNS is more favorable for increasing e–h separation efficiency as compared to the interaction between benzene and TNS-F. The longer fluorescence lifetime of TNS than TNS-F in benzene vapor results in its higher photocatalytic activity for benzene photodegradation (Fig. 4B).

3.5. DFT calculation

The interaction between reactant and TiO_2 was theoretically investigated by density functional theory (DFT) calculation. FTIR (Fig. S6) and XPS (Fig. 3) show that TNS contains many hydroxyl groups and TNS-F contains both hydroxyl and surface Ti-F groups. Therefore, two H_2O molecules and two HF molecules adsorbed on exposed {0 0 1} surface of TiO_2 slab ($Ti_{27}O_{54}$) are used as starting model for the structure optimization of the F-free TiO_2 slab and F-modified TiO_2 slab, respectively. Thus, the optimized F-free TiO_2 slab ($Ti_{27}O_{52}(OH)_4$) contains four surface hydroxyl groups (Fig. S7), while the optimized F-modified TiO_2 slab ($Ti_{27}O_{52}F_2(OH)_2$) contains two hydroxyl groups and two surface Ti–F groups (Fig. S7). This result reveals that water molecule is dissociatively adsorbed on the {0 0 1} facets, which is in agreement with previous report [47]. HF molecule is also dissociatively adsorbed on the {0 0 1} facets to form surface Ti-F bond and hydroxyl group. Then, the structure optimization is performed for the systems of acetone and benzene molecule adsorbed on the optimized F-free TiO_2 slab and F-modified TiO_2 slab, respectively. The adsorption energy and density of states (DOS) are calculated for the structure optimized systems of benzene and acetone adsorbed on exposed {0 0 1} surface of F-free and F-modified TiO_2 slab. The adsorption energy of acetone on F-modified TiO_2 slab (−0.33 eV) (Fig. 7A) is lower than that of acetone on F-free TiO_2 slab (−0.24 eV) (Fig. 8), indicating a more strong adsorption of acetone on F-modified TiO_2 than F-free TiO_2. The strong adsorption is further confirmed by the elongation of O=C bond in acetone adsorbed on F-modified TiO_2 slab (1.2458 Å) as compared to that in acetone adsorbed on F-free TiO_2 slab (1.2306 Å) and in free acetone(1.2275 Å). TDOS analysis reveals that the adsorption of acetone on the F-modified TiO_2 slab leads to

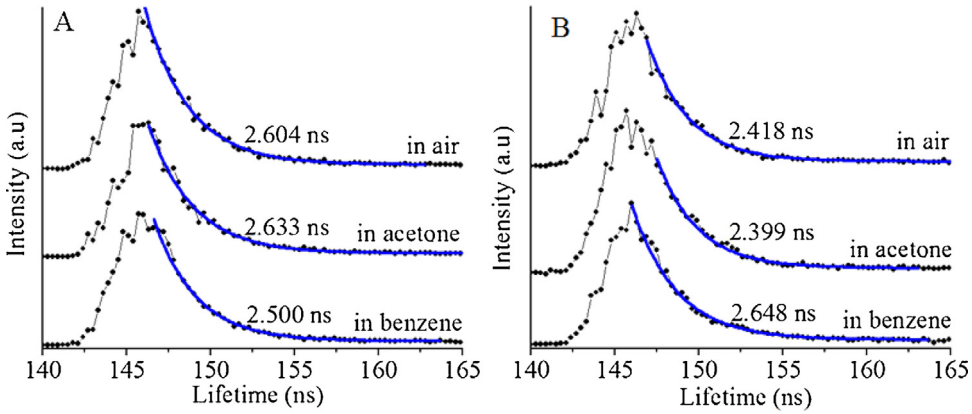

Fig. 6. Fluorescence emission decay recorded at 430 nm for TNS-F (A) and TNS (B) in different atmosphere using 337 nm excitation. The blue dotted lines are the corresponding fitting curve.

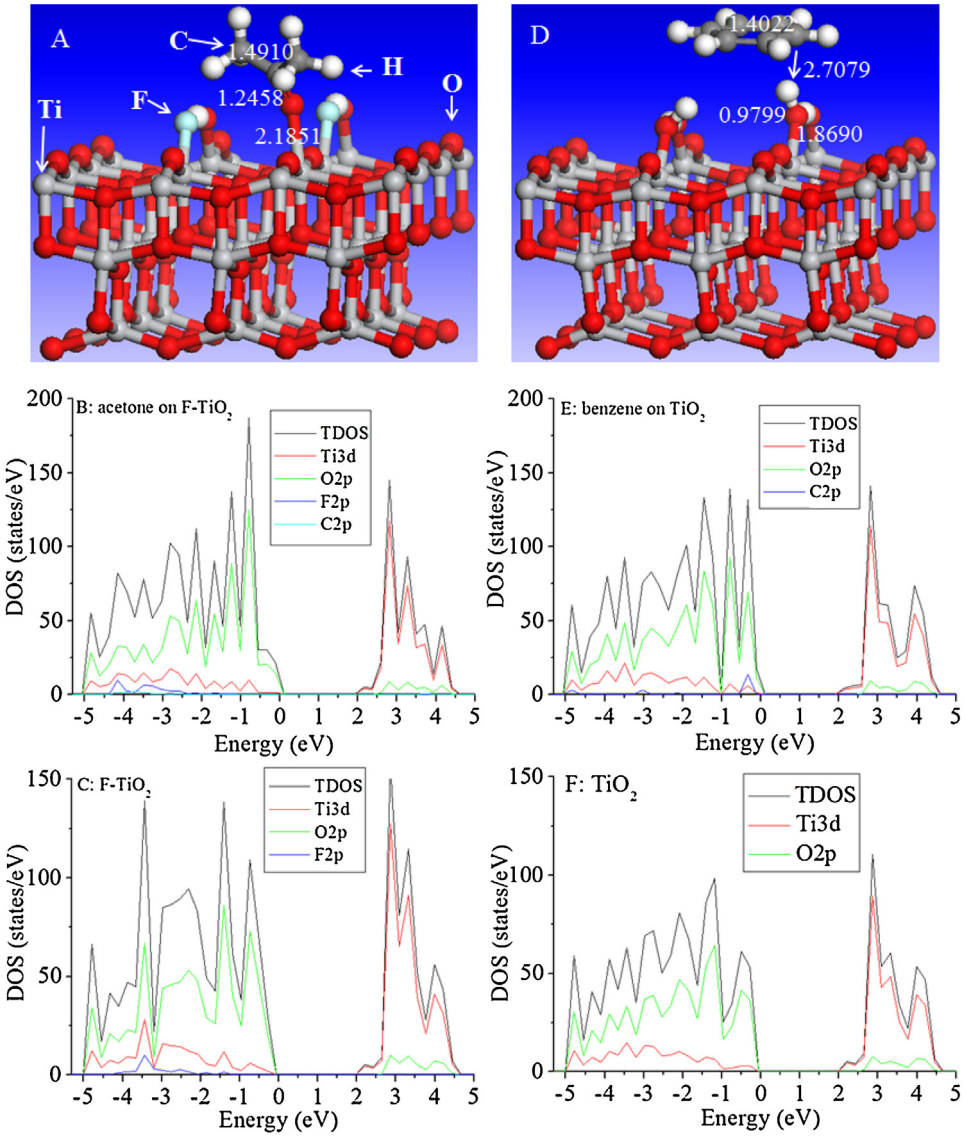

Fig. 7. Optimized structure and DOS of acetone adsorbed on the {0 0 1} surface of F-modified TiO_2 slab (A and B) and benzene adsorbed on the {0 0 1} surface of F-free TiO_2 slab (D and E), and DOS of F-modified TiO_2 slab (C) and F-free TiO_2 slab (F): data in A and D are bond length.

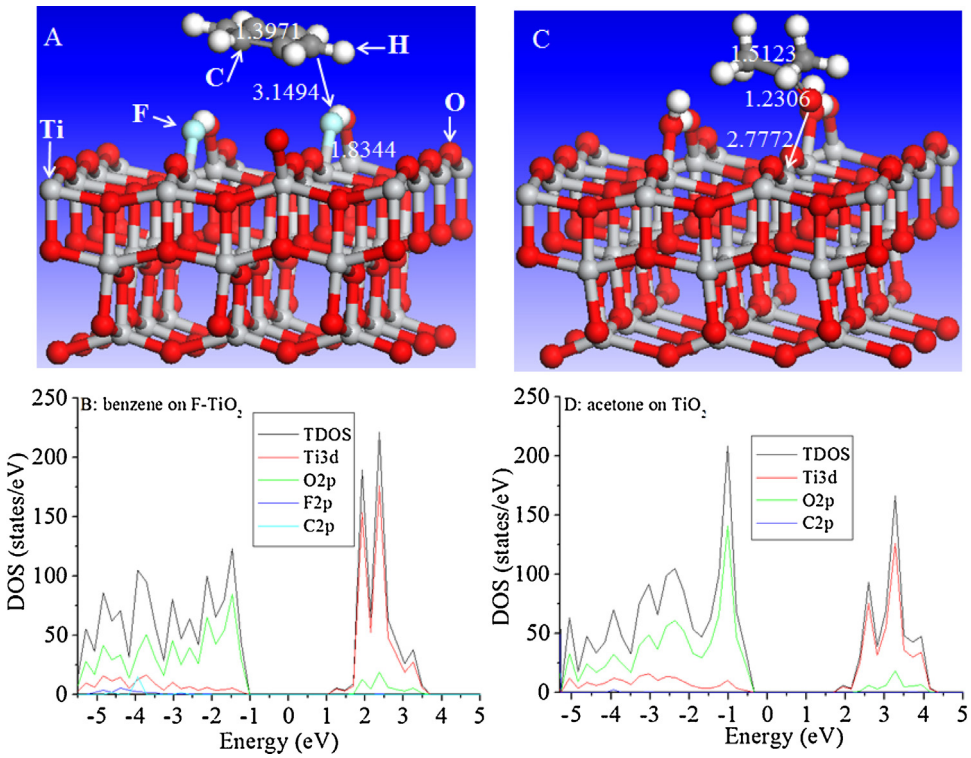

Fig. 8. Optimized structure and DOS of benzene adsorbed on the {0 0 1} surface of F-modified TiO_2 slab (A and B) and acetone adsorbed on the {0 0 1} surface of F-free TiO_2 slab (C and D): data in A and C are bond length.

a decrease of band gap from 2.02 to 1.85 eV as compared to the F-modified TiO_2 slab (Fig. 7B and C). This result accounts for the efficient visible photocatalytic activity for the acetone photodegradation on TNS-F (Fig. 4C). Enlarged PDOS indicates that the upper part of the valence band for the acetone adsorbed on F-modified TiO_2 has contribution of O2p and C2p in acetone (Fig. S8). This result reveals that upon UV excitation, the photogenerated holes in the valence band of F-modified TiO_2 can transfer to O2p and C2p of adsorbed acetone, thus increasing the separation efficiency of e–h. This explains the higher photocatalytic activity for the acetone photodegradation on TNS-F than that on TNS (Fig. 4A).

For benzene adsorption, the lower adsorption energy of F-free TiO_2 (−0.21 eV) than F-modified TiO_2 (0.029 eV) indicates a more strong adsorption of benzene on the former. The adsorption of benzene on F-free TiO_2 slab leads to a decrease of their band gap from 2.02 to 1.85 eV as compared to F-free TiO_2 slab (Fig. 7E and F). In contrast, the band gap remains unchanged for the adsorption of benzene on F-modified TiO_2 (Fig. 8A and B). This explains why TNS has efficient visible photocatalytic activity for the benzene photodegradation (Fig. 4D). For benzene adsorbed on F-modified TiO_2, C2p DOS of benzene is far below the top of valence band (Fig. 8B). Interestingly, for benzene adsorbed on F-free TiO_2, C2p DOS of benzene shifts to the upper part of valence band (Fig. 7E). This result reveals that upon UV excitation, the photogenerated holes in the valence band of F-free TiO_2 can transfer to C2p of adsorbed benzene, thus increasing the separation efficiency of e–h. This explains the higher photocatalytic activity for the benzene photodegradation on TNS than that on TNS-F (Fig. 4B). These DFT calculation results clearly indicate the strong interaction between benzene and F-free TiO_2 nanosheets. The strong interaction is further confirmed by the elongation of C=C bond in benzene adsorbed on F-free TiO_2 slab (1.4022 Å, Fig. 7D) as compared to that in benzene adsorbed on F-modified TiO_2 slab (1.3971 Å, Fig. 8A).

The interaction between toluene and F-free TiO_2 or F-modified TiO_2 was also theoretically investigated by DFT calculation. We obtain the result similar to the interaction between benzene and F-free TiO_2 or F-modified TiO_2. The adsorption of toluene on F-free TiO_2 slab leads to a decrease of their band gap from 2.02 to 1.80 eV as compared to F-free TiO_2 slab (Fig. S9C). In contrast, the band gap remains unchanged for the adsorption of toluene on F-modified TiO_2 (Fig. S9D). This explains why TNS has the photocatalytic activity for the toluene photodegradation under the visible irradiation (Fig. S3). This result indicates that there is strong interaction between toluene and F-free TiO_2 nanosheets. The strong interaction is further confirmed by the elongation of C=C bond in toluene adsorbed on F-free TiO_2 slab (1.4010 Å, Fig. 9S) as compared to that in toluene adsorbed on F-modified TiO_2 slab (1.3942 Å, Fig. 9S).

As can be seen from Figs. 7 and 8, and Fig. 9S, there is a considerable shift of DOS for benzene adsorbed on F-modified TiO_2 slab (Fig. 8B) and toluene adsorbed on F-modified TiO_2 slab (Fig. S9D) as compared to F-modified TiO_2 slab (Fig. 7C). The main reason is as follows: benzene or toluene with conjugate ring adsorbed on TiO_2 slab is equivalent to inducing a potential (U) on TiO_2, thus resulting in the shift of their DOS [48]. However, there is no obvious shift of DOS for benzene adsorbed on F-free TiO_2 slab (Fig. 7E) and toluene adsorbed on F-free TiO_2 slab (Fig. S9B) as compared to F-free TiO_2 slab (Fig. 7F). This is due to the fact that the strong interaction between F-free TiO_2 slab and benzene or toluene lead to a considerable shift of C2p in benzene or toluene to the upper part of valence band (Figs. 7 E and 8 B, Fig. 9SB and 9SD) as compared to benzene or toluene adsorbed on F-modified TiO_2 slab. The strong interaction counteracts the potential effect of benzene or toluene with conjugate ring on F-free TiO_2 slab.

The major scientific issues for TiO_2 photocatalysis are how to improve its photocatalytic efficiency and extend its photocatalytic

response to visible region. The reported strategies for the former involve: forming a rutile/anastase junction [49,50], improving its specific surface area through preparing various nanostructured TiO_2 [51–53], increasing surface/bulk defect ratio or crystallinity of TiO_2 nanocrystals [46,54], fluorination of TiO_2 [38–43], controlling the exposed facets (e.g.,{0 0 1}) of TiO_2 nanocrystals [12–30], utilizing the effect of slow photon and multiple scattering in TiO_2 photonic crystal, etc. [55,56] The reported strategies for the latter involve narrowing the band gap of TiO_2 by doping or co-doping diverse metals and nonmetals [57–61], Ti^{3+} self-doping [62,63], and so on. These reported strategies were realized through controlling the physicochemical properties and microstructures of TiO_2-based photocatalysts without focusing on the effect of organic pollutants on the photocatalytic performance. The present work provides a novel strategy of considerably enhancing the photocatalytic activity and developing efficient visible photocatalysis for environmental cleanup through controlling the interaction between organic pollutants and TiO_2. This can be done by the surface modification of anatase TiO_2 nanosheets with exposed {0 0 1} facets and choosing appropriate organic pollutant.

Conclusion

In summary, a novel and important effect of the interaction between the reactants and TiO_2 nanosheets with exposed {0 0 1} facets on photocatalysis is found. The interaction depends on the property of reactants as well as the surface physicochemical property of TiO_2. It affects both the separation efficiency of the photogenerated charge carriers from TiO_2 to the reactants and their band gap characteristics. The strong interaction not only reverses the photocatalytic activity of F-free TiO_2 nanosheets and F-modified TiO_2 nanosheets, but also induces efficient visible photocatalytic activity. The surface modification of TiO_2 nanosheets with F increases the interaction with acetone as compared to F-free TiO_2 nanosheets, resulting in the higher photocatalytic activity and the visible photocatalytic activity of F-modified TiO_2 for the acetone photodegradation. On the other hand, F-free TiO_2 nanosheets have more strong interaction with benzene or toluene than F-modified TiO_2 nanosheets, resulting in the photocatalytic activity of the former higher than the later and the visible photocatalytic activity of the former for the photodegradation of benzene or toluene. The findings in the present work provide fundamental insight into the effect of the interaction, and open up a novel strategy for considerably enhancing photocatalytic efficiency and developing visible photocatalysis for environmental cleanup or selective purification through controlling the interaction. We believe that the effect may also be applicable to other photocatalytic nanocrystals with exposed facets of high surface energy.

Acknowledgements

This work was supported by National Natural Science Foundation of China (21473127, 21273169) and Research and Development Project of Hubei Province (2013BAA045).

Appendix A. Supplementary data

Supplementary data associated with this article can be found, in the online version, at http://dx.doi.org/10.1016/j.apcatb.2015.08.034.

References

[1] Y. Ma, Y.Z. Li, M.Y. Mao, J.J. Hou, M. Zeng, X.J. Zhao, J. Mater. Chem. A 3 (2015) 5509–5516.
[2] X.B. Chen, S.S. Mao, Chem. Rev. 107 (2007) 2891–2959.
[3] A.L. Linsebigler, G.Q. Lu, J.T. Yates Jr., Chem. Rev. 95 (1995) 735–758.
[4] H.G. Yang, C.H. Sun, S.Z. Qiao, J. Zou, G. Liu, S.C. Smith, H.M. Cheng, G.Q. Lu, Nature 453 (2008) 638–642.
[5] S.W. Liu, J.G. Yu, M. Jaroniec, Chem. Mater. 23 (2011) 4085–4093.
[6] Y.Q. Dai, C.M. Cobley, J. Zeng, Y.M. Sun, Y.N. Xia, Nano. Lett. 9 (2009) 2455–2459.
[7] C.Z. Wen, J.Z. Zhou, H.B. Jiang, Q.H. Hu, S.Z. Qiao, H.G. Yang, Chem. Commun. 47 (2011) 4400–4402.
[8] X.G. Han, Q. Kuang, M.S. Jin, Z.X. Xie, L. Zheng, J. Am. Chem. Soc. 131 (2009) 3152–3153.
[9] J.G. Yu, J.X. Low, W. Xiao, P. Zhou, M. Jaroniec, J. Am. Chem. Soc. 136 (2014) 8839–8842.
[10] T.R. Gordon, M. Cargnello, T. Paik, F. Mangolini, R.T. Weber, P. Fornasiero, C.B. Murray, J. Am. Chem. Soc. 134 (2012) 6751–6761.
[11] Y.F. Li, Z.P. Liu, L.L. Liu, W.G. Gao, J. Am. Chem. Soc. 132 (2010) 13008–13015.
[12] H.B. Jiang, Q. Cuan, C.Z. Wen, J. Xing, D. Wu, X.Q. Gong, C.Z. Li, H.G. Yang, Angew. Chem. Int. Ed. 50 (2011) 3764–3768.
[13] N. Roy, Y. Sohn, D. Pradhan, ACS Nano 7 (2013) 2532–2540.
[14] (a) J.Y. Chen, G.Y. Li, H.M. Zhang, P. Liu, H.J. Zhao, T.C. An, Catal. Today 224 (2014) 216–224;
(b) T.C. An, J.Y. Chen, X. Nie, G.Y. Li, H.M. Zhang, X.L. Liu, H.J. Zhao, ACS Appl. Mater. Interfaces 4 (2012) 5988–5996.
[15] T. Tachikawa, S.T. Yamashitam Majima, J. Am. Chem. Soc. 133 (2011) 7197–7204.
[16] Z.F. Bian, J. Zhu, J. Wen, F.L. Cao, Y.N. Huo, X.F. Qian, Y. Cao, M.Q. Shen, H.X. Li, Y.F. Lu, Angew. Chem. Int. Ed. 123 (2011) 1137–1140.
[17] J. Zhu, J.G. Wang, F.J. Lv, S.X. Xiao, C. Nuckolls, H.X. Li, J. Am. Chem. Soc. 135 (2013) 4719–4721.
[18] S.W. Liu, J.G. Yu, M. Jaroniec, J. Am. Chem. Soc. 132 (2010) 11914–11916.
[19] G. Liu, H.G. Yang, X.W. Wang, L. Cheng, J. Pan, G.Q. Lu, H.M. Cheng, J. Am. Chem. Soc. 131 (2009) 12868–12869.
[20] S.F. Xie, X.G. Han, Q. Kuang, J. Fu, L. Zhang, Z.X. Xie, L.S. Zheng, Chem. Commun. 47 (2011) 6722–6724.
[21] B.H. Wu, C.Y. Guo, N.F. Zheng, Z.X. Xie, G.D. Stucky, J. Am. Chem. Soc. 130 (2008) 17563–17567.
[22] T. Tachikawa, N. Wang, S. Yamashita, S.C. Cui, T. Majima, Angew. Chem. Int. Ed. 49 (2010) 8593–8597.
[23] M. Ferus, L. Kavan, M. Zukalova, A. Zukal, M. Klementova, S. Civis, J. Phys. Chem. C 118 (2014) 26845–26850.
[24] J.Y. Zheng, S.H. Bao, Y. Guo, P. Jin, ACS Appl. Mater. Interfaces 6 (2014) 5940–5946.
[25] L. Gu, J.Y. Wang, H. Cheng, Y.Z. Zhao, L.F. Liu, X.J. Han, ACS Appl. Mater. Interfaces 5 (2013) 3085–3093.
[26] Y.B. Zhao, Y.F. Zhang, H.W. Liu, H.W. Ji, W.H. Ma, C.C. Chen, H.Y. Zhu, J.C. Zhao, Chem. Mater. 26 (2014) 1014–1018.
[27] A.S. Ichimura, B.M. Mack, S.M. Usmani, D.G. Mars, Chem. Mater. 24 (2012) 2324–2329.
[28] Z.F. Bian, T. Tachikawa, T. Majima, J. Phys. Chem. Lett 3 (2012) 1422–1427.
[29] T. Sun, Y. Wang, H.M. Zhang, P.R. Liu, H.J. Zhao, J. Colloid Interface Sci. 454 (2015) 180–186.
[30] Q.J. Xiang, K.L. Lv, J.G. Yu, Appl. Catal. B 96 (2010) 557–564.
[31] L. Ren, Y.Z. Li, J.T. Hou, X.J. Zhao, C.X. Pan, ACS Appl. Mater. Interfaces 6 (2014) 1608–1615.
[32] J.T. Hou, Y.Z. Li, M.Y. Mao, X.J. Zhao, Y.Z. Yue, Nanoscale 6 (2014) 15048–15058.
[33] J.T. Hou, L.L. Liu, Y.Z. Li, M.Y. Mao, H.Q. Lv, X.J. Zhao, Environ. Sci. Technol. 47 (2013) 13730–13736.
[34] G. Kresse, J. Hafner, Phys. Rev. B 47 (1993) 558–561.
[35] G. Kresse, J. Hafner, Phys. Rev. B 49 (1994) 14251–14269.
[36] G. Kresse, J. Furthmuller, Comput. Mater. Sci. 6 (1996) 15–50.
[37] P.E. Blochl, Phys. Rev. B 50 (1994) 17953–17979.
[38] S.W. Liu, J.G. Yu, B. Cheng, M. Jaroniec, Adv. Colloid Interface Sci. 173 (2012) 35–53.
[39] C. Minero, G. Mariella, V. Maurino, E. Pelizzetti, Langmuir 16 (2000) 2632–2641.
[40] H. Park, Y. Park, W. Kim, W.Y. Choi, J. Photochem. Photobiol. C 15 (2013) 1–20.
[41] H. Park, W. Choi, J. Phys. Chem. 108 (2004) 4086–4093.
[42] K.L. Lv, Y.M. Xu, J. Phys. Chem. B 110 (2006) 6204–6212.
[43] J.W. Tang, H.D. Quan, J.H. Ye, Chem. Mater. 19 (2007) 116–122.
[44] (a) Y.B. Luan, L.Q. Jing, Y. Xie, X.J. Sun, Y.J. Feng, H.G. Fu, ACS Catal. 3 (2013) 1378–1385;
(b) Y. Cao, L.Q. Jing, X. Shi, J.R. Luan, J.W. Tang, H.G. Fu, Phys. Chem. Chem. Phys. 14 (2012) 8530–8536.
[45] L. Thompson, J.T. Yates Jr., Chem. Rev. 106 (2006) 4428–4453.
[46] M. Kong, Y.Z. Li, X. Chen, T.T. Tian, P.F. Fang, F. Zheng, X.J. Zhao, J. Am. Chem. Soc. 133 (2011) 16414–16417.
[47] A. Selloni, Nat. Mater. 7 (2008) 613–615.
[48] N. Li, K.L. Yao, Z.Y. Sun, L. Zhu, G.Y. Gao, J. Appl. Phys. 109 (2011) 083715.
[49] A. Di Paola, M. Bellardita, R. Ceccato, L. Palmisano, F. Parrino, J. Phys. Chem. C 113 (2009) 15166–15174.
[50] T. Kawahara, Y. Konishi, H. Tada, N. Tohge, J. Nishii, S. Ito, Angew. Chem. Int. Ed. 41 (2002) 2811–2813.
[51] J.C. Yu, L.Z. Zhang, J.G. Yu, Chem. Mater. 14 (2002) 4647–4653.
[52] T. Peng, D. Zhao, K. Dai, W. Shi, K. Hirao, J. Phys. Chem. B 109 (2005) 4947–4952.

[53] W.Y. Dong, Y.J. Sun, C.W. Lee, W.M. Hua, X.C. Lu, Y.F. Shi, S.C. Zhang, J.M. Chen, D.Y. Zhao, J. Am. Chem. Soc. 129 (2007) 13894–13904.
[54] W. Zhou, F.F. Sun, K. Pan, G.H. Tian, B.J. Jiang, Z.Y. Ren, C.G. Tian, H.G. Fu, Adv. Funct. Mater. 21 (2011) 1922–1930.
[55] Y.Z. Li, T. Kunitake, S. Fujikawa, J. Phys. Chem. B 110 (2006) 13000–13004.
[56] J.I.L. Chen, G. von Freymann, S.Y. Choi, V. Kitaev, G.A. Ozin, Adv. Mater. 18 (2006) 1915–1919.
[57] S.U.M. Khan, M. Al-Shahry, W.B. Ingler Jr., Science 297 (2002) 2243–2245.
[58] R. Asahi, T. Morikawa, T. Ohwaki, K. Aoki, Y. Taga, Science 293 (2001) 269–271.
[59] W. Zhao, W.H. Ma, C. Chen, J.C. Zhao, Z. Shuai, 126, J. Am. Chem. Soc. (2004) 4782.
[60] X.B. Chen, C. Burda, J. Am. Chem. Soc. 130 (2008) 5018–5019.
[61] N. Shi, X.H. Li, T.X. Fan, H. Zhou, J.A. Ding, D. Zhang, H.X. Zhu, Energy Environ. Sci. 4 (2011) 172–180.
[62] F. Zuo, L. Wang, T. Wu, Z.Y. Zhang, D. Borchardt, P.Y. Feng, J. Am. Chem. Soc. 132 (2010) 11856–11857.
[63] W.Z. Fang, M.Y. Xing, J.L. Zhang, Appl. Catal. B 160 (2014) 240–246.